AGU PUBLICATIONS

Geophysical Research Letters

RESEARCH LETTER
10.1002/2017GL073777

Key Points:
- CryoSat-2 delivers new data along the Norwegian coast, in areas previously not monitored by altimetry
- CryoSat-2 mean dynamic topographies agree on the 3–5 cm level with both tide-gauge geodetic and ocean mean dynamic topographies
- By comparison of geodetic and ocean mean dynamic topographies, we are able to detect errors in the coastal marine gravity field

Supporting Information:
- Supporting Information S1

Correspondence to:
M. Idžanović,
martina.idzanovic@nmbu.no

Citation:
Idžanović, M., V. Ophaug, and O. B. Andersen (2017), The coastal mean dynamic topography in Norway observed by CryoSat-2 and GOCE, *Geophys. Res. Lett.*, *44*, 5609–5617, doi:10.1002/2017GL073777.

Received 13 JAN 2017
Accepted 18 MAY 2017
Accepted article online 24 MAY 2017
Published online 11 JUN 2017

The coastal mean dynamic topography in Norway observed by CryoSat-2 and GOCE

Martina Idžanović[1], Vegard Ophaug[1], and Ole Baltazar Andersen[2]

[1]Faculty of Science and Technology, Norwegian University of Life Sciences (NMBU), Ås, Norway, [2]DTU Space, Technical University of Denmark, Kgs. Lyngby, Denmark

Abstract New-generation synthetic aperture radar altimetry, as implemented on CryoSat-2, observes sea surface heights in coastal areas that were previously not monitored by conventional altimetry. Therefore, CryoSat-2 is expected to improve the coastal mean dynamic topography (MDT). However, the MDT remains highly reliant on the geoid. Using new regional geoid models as well as CryoSat-2 data, we determine three geodetic coastal MDT models in Norway and validate them against independent tide-gauge observations and the operational coastal ocean model NorKyst800. The CryoSat-2 MDTs agree on the ∼3–5 cm level with both tide-gauge geodetic and ocean MDTs along the Norwegian coast. In addition, we compute geostrophic surface currents to help identifying errors in the geoid models. We find that even though the regional geoid models are all based on the latest satellite gravity data as provided by GOCE, the resulting circulation patterns differ. We demonstrate that some of these differences are due to erroneous or lack of marine gravity data. This suggests that there is significant MDT signal at spatial scales beyond GOCE, and that the geodetic approach to MDT determination benefits from the additional terrestrial gravity information provided by a regional geoid model. We also find that the border of the geographical mode mask of CryoSat-2 coincides with the Norwegian Coastal Current, making it challenging to distinguish between artifacts in the CryoSat-2 observations during mode switch and ocean signal.

1. Introduction

Although satellite altimetry is a mature technique, observing the sea surface height (SSH) globally with an accuracy of a few centimeters [*Chelton et al.*, 2001], numerous effects degrade the observations in the coastal zone [*Vignudelli et al.*, 2011]. For example, the radar footprint is contaminated by land and bright targets, and the range and geophysical corrections become difficult to model. The rugged Norwegian coast presents a further challenge, where the Norwegian Coastal Current (NCC) typically falls into a zone where conventional altimeters do not deliver reliable observations [*Ophaug et al.*, 2015].

CryoSat-2 (CS2) [*Wingham et al.*, 2006] carries a synthetic aperture interferometric radar altimeter (SIRAL) which can operate in synthetic aperture radar (SAR), interferometric SAR (SARIn), and conventional low-resolution (LR) modes. CS2 uses a geographical mode mask to decide which mode to operate in [*European Space Agency and Mullard Space Science Laboratory-University College London*, 2012]. The SAR mode improves the along-track resolution to ∼300 m through a complex Doppler processing chain. The SARIn mode has a similar resolution and also measures the phase difference of the backscattered signal at two antennas, from which the position of any backscattered point may be derived. Thus, the SARIn mode may help in discriminating and mitigating land contamination signals from off-nadir land targets (e.g., steep cliffs) [*Armitage and Davidson*, 2014] in the Norwegian coastal zone.

The geodetic dynamical ocean topography (DOT) is computed by [e.g., *Pugh and Woodworth*, 2014]

$$\mathrm{DOT} = h - N, \tag{1}$$

where h is the ellipsoidal height of sea level and N is the geoid height, all referring to the same reference ellipsoid. If we average h over a specific time period, equation (1) will give the mean dynamic topography (MDT) for that period as a difference between the mean sea surface (MSS) and the geoid. Using equation (1), the MDT has a high dependence on the geoid model.

In this work we use three state-of-the-art regional geoid models as well as CS2 data in the Norwegian coastal zone and determine coastal MDT models by equation (1). Our main goal is to validate the three CS2 MDTs against tide-gauge observations and the state-of-the-art operational coastal numerical ocean model NorKyst800.

Typically, geodesists assess the quality of regional geoid models by external validation against geometrically determined geoid heights on land, at sites observed by both Global Navigation Satellite Systems (GNSS) and leveling [*Denker*, 2013]. This approach is not ideal for assessing the regional geoid model over marine areas [*Ophaug et al.*, 2015]. Instead, we compute geostrophic surface currents from our CS2 MDTs to help identifying errors in the marine gravity field that are emphasized through the differentiation.

We compare coastal MDTs determined by the methodically different approaches of geodesy and oceanography. This work is a natural extension of such comparisons along different coasts [e.g., *Woodworth et al.*, 2012; *Higginson et al.*, 2015; *Hughes et al.*, 2015; *Lin et al.*, 2015; *Woodworth et al.*, 2015]. In particular, this work builds upon the benchmark comparison of geodetic and ocean MDTs along the Norwegian coast presented by *Ophaug et al.* [2015].

Section 2 describes the data and methods we use to determine the CS2 MDTs and validate them. The CS2 data and MDT computation is described in section 2.1. Section 2.2 presents the data used to validate the CS2 MDTs, specifically the tide-gauge geodetic MDT (section 2.2.1) and the NorKyst800 ocean MDT (section 2.2.2). In section 3 we assess the CS2 MDTs by comparing geodetic and ocean MDT profiles at tide gauges, as well as comparing flow patterns of the CS2 MDTs and NorKyst800. Finally, we discuss our results and give some concluding remarks in section 4.

2. Data and Methods

2.1. CryoSat-2 MDT

While equation (1) seems computationally simple, it is important that h and N cover the same wavelengths. Typically, when using satellite-only geoid models, h contains small-scale features that N lacks, requiring a suitable filtering of h to reduce the error of N.

In order to resolve the smallest spatial scales of the gravity field and thus reduce the filtering need, we have referenced ellipsoidal sea level to three regional geoid models, namely, the operational regional geoid model for Norway, NMA2014, as described in *Ophaug et al.* [2015], the Nordic Geodetic Commission NKG2015 model [*Ågren et al.*, 2016], and the European Gravimetric Geoid EGG2015 [*Denker*, 2016], see supporting information Table S1. All are based on fifth release data from the European Space Agency (ESA) satellite gravity mission Gravity and steady-state Ocean Circulation Explorer (GOCE) [*Drinkwater et al.*, 2003]. The geoid heights were transformed from the zero-tide system to the mean tide (MT) system using *Ekman* [1989, equation (17)]. They refer to the WGS84 ellipsoid.

CS2 operates in LR mode (LRM) over most of the Norwegian Sea, and in SAR mode in the North Sea and Skagerrak area. It switches to SARIn mode in the Norwegian coastal areas. SARIn data points are available in a zone stretching out ~40 km off the Norwegian coast (Figure 3b). Thus, we have used SSH observations obtained in all three modes in this work.

The LR and SAR mode data were obtained through the Radar Altimeter Database System (RADS) [*Scharroo et al.*, 2013a]. It contains 1 Hz values referring to the TOPEX ellipsoid and was referenced to WGS84 by considering an average difference of 0.686 m between WGS84 and TOPEX [*Ophaug et al.*, 2015]. RADS provides SAR mode observations as so-called pseudo-LRM observations; i.e., they are reduced SAR observations using an incoherent processing of the pulse-limited echoes, similar to the conventional LRM processing [*Scharroo et al.*, 2013b]. Therefore, we will refer to all RADS data as LRM data in the following.

SARIn mode observations were obtained from the ESA Grid Processing On Demand (GPOD) CryoSat-2 service [*Benveniste et al.*, 2016], which provides CS2 data in two modes, Level 1 (L1) and Level 2 (L2). The data processing is based on the L2 data set, as well as the 1 Hz L1b data set, which is retracked using the SAR Altimetry Mode Studies and Applications (SAMOSA) 2 physical retracker [*Ray et al.*, 2015]. The SARIn off-nadir range correction was applied in the processing [*Armitage and Davidson*, 2014; *Abulaitijiang et al.*, 2015]. To obtain a reliable temporal mean (see below), we let our CS2 data set cover the 2010–2015 period. This slightly

translates the temporal mean epoch by a year as compared to the tide-gauge geodetic and ocean MDTs. The time difference corresponds to a negligible difference of ∼2 mm in SSH due to regional sea-level rise [*Simpson et al.*, 2015].

As opposed to the LRM data obtained from RADS, no editing or quality assessment has been performed on the SARIn data. We have considered standard range and geophysical corrections for both LRM and SARIn data sets, see supporting information Table S2 [*Cartwright and Tayler*, 1971; *Cartwright and Edden*, 1973; *Wahr*, 1985]. We first removed all observations over land, giving 21,535 data points over the ocean. Next, by visual inspection of the data set, we identified a bias in the SARIn data and removed outliers within 0 m $\geq N \geq$ 0.6 m. In addition, we performed a within-track outlier removal by multiple Student's t test (two-tailed, with $\alpha = 0.05$) [e.g., *Koch*, 1999]. This two-step outlier removal led to a ∼45% reduction in the SARIn data points.

Geoid heights from each geoid model were interpolated to the location of CS2 SSH observations, from which they were subsequently subtracted. Due to the geodetic orbit of CS2, we need to spatially average the DOT values to get a temporal mean and avoid striping effects. Therefore, all observations were combined and averaged in 20 × 20 km bins and interpolated onto a regular grid with 30-arc sec resolution, within an area delimited by 55.8092° $\leq \varphi \leq$ 73° and 0° $\leq \lambda \leq$ 34°. The interpolation was done using least-squares collocation [*Moritz*, 1980], see supporting information Text S1 [*Forsberg and Tscherning*, 2008; *Moritz*, 1980; *Wunsch and Stammer*, 1998]. CS2 MDTs based on NKG2015, EGG2015, and NMA2014 will be referred to as $C2_{NKG}$, $C2_{EGG}$, and $C2_{NMA}$ in the following.

We have chosen to compare flow patterns in the form of geostrophic surface currents, see supporting information Text S1. Under the geostrophic assumption we look at the surface component of the flow. We are aware that the geostrophic assumption is not necessarily valid close to the coast [e.g., *Lin et al.*, 2015]. However, we determine the currents mainly to facilitate our assessment of the regional geoid models, as any error in the geoid will be emphasized through the differentiation.

2.2. Validation Data

2.2.1. Tide-Gauge MDT

We have considered a subset of 19 tide-gauges (TGs) on the Norwegian mainland in this work, see Figure 1a and supporting information Table S3. Thereby, we have omitted four TGs due to their location well inside fjords that are not sufficiently covered by altimetry data [*Ophaug et al.*, 2015]. Monthly sea-level observations for 2012–2015 were obtained from the Permanent Service for Mean Sea Level (PSMSL) [*Holgate et al.*, 2013] at http://www.psmsl.org/data/obtaining/. Local pressure observations with 10-min temporal resolution have been obtained from the database of the Norwegian Mapping Authority (NMA) (K. Breili, personal communication, 2016). As Mausund data are not yet available at PSMSL, these data were obtained from the NMA database. The pressure observations were used to correct sea level for the ocean's inverted barometer (IB) effect, following the approach of *Idžanović et al.* [2016].

The sea-level observations are given as heights H in the national height system, NN2000. As none of the considered TGs have been observed directly by GNSS with sufficient accuracy, we have derived ellipsoidal heights h of mean sea level (MSL) using the Norwegian height reference surface HREF2016A [*Solheim*, 2000], and the simple relation $h = H +$ HREF, following the approach of *Ophaug et al.* [2015]. NKG2015, EGG2015, and NMA2014 were linearly interpolated to the tide-gauge sites, and by equation (1), TG_{NKG}, TG_{EGG}, and TG_{NMA} were determined, respectively.

2.2.2. NorKyst800

We have considered the operational coastal ocean model of MET Norway, NorKyst800, based on the Regional Ocean Modeling System (ROMS) [*Haidvogel et al.*, 2008]. It was obtained from http://met.no/Hav_og_is/English/Access_to_data/, where it is available in the form of daily mean values since July 2nd 2012.

NorKyst800 uses a polar stereographic grid delimited by 55.8092° $\leq \varphi \leq$ 75.2419° and −1.5651° $\leq \lambda \leq$ 38.0339°, at an eddy-resolving resolution of 800 m. The applied version of NorKyst800 uses atmospheric forcing by *Røed and Debernard* [2004] and additionally considers a sea ice component [*Budgell*, 2005]. It includes tidal forcing from the global TPXO model [*Egbert and Erofeeva*, 2002] and freshwater runoff from a hydrological model discharge at 256 main catchment areas.

To make our validation easier, NorKyst800 was resampled to a regular grid with 30-arc sec resolution using the NEARNEIGHBOR routine of the Generic Mapping Tools (GMT) [*Wessel et al.*, 2013]. As NorKyst800 is forced by

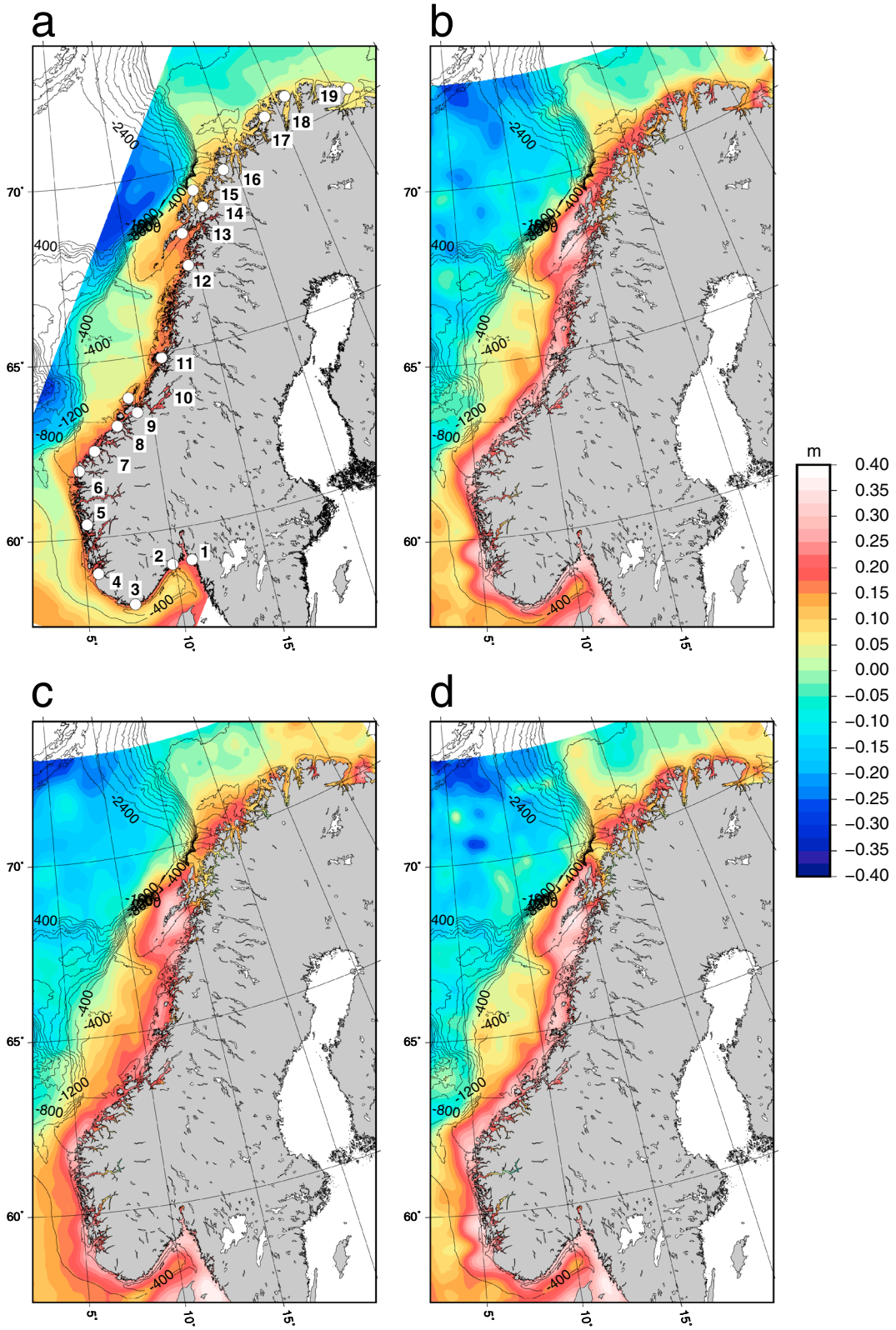

Figure 1. Coastal MDTs in Norway; (a) ocean, based on NorKyst800, and geodetic, based on (b) $C2_{NKG}$, (c) $C2_{EGG}$, and (d) $C2_{NMA}$. The mean value, given in supporting information Table S4, has been removed in all cases. The tide gauges considered in this work are shown in Figure 1a, for which a code is given in Figure 2. In all (Figures 1a–1d), 400 m isobaths from the 2014 General Bathymetric Charts of the Oceans (GEBCO) [*Weatherall et al.*, 2015] grid are shown.

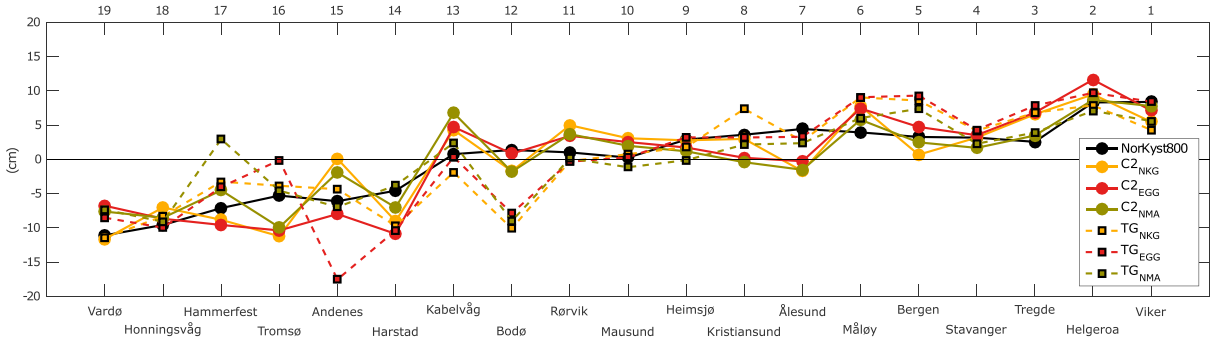

Figure 2. Tide-gauge MDT profiles using geodetic and ocean estimates, arranged and numbered from north to south, as shown in Figure 1a. For all profiles the mean value has been removed. Tide gauge (TG) names and IDs are given on the bottom and top *x* axis, respectively.

atmospheric pressure, it includes the IB effect. We corrected NorKyst800 for the IB effect by applying *Wunsch and Stammer* [1997, equation (1)] to a 0.25° × 0.25° mean sea-level pressure field for the 2012–2015 period, obtained from the European Centre for Medium-Range Weather Forecasts (ECMWF) Interim Reanalysis (ERA Interim) [*Dee et al.*, 2011].

3. Results

The CS2 MDTs (Figures 1b–1d) are generally consistent with NorKyst800 (Figure 1a), with slightly larger values in the coastal zone (up to ~40 km off the coast) and smaller values to the open ocean. The general pattern of the Norwegian Sea circulation is evident in all MDTs; we trace the Norwegian Atlantic Current (NwASC) northward and observe its branching at the Barents Sea Opening around 72°N, as well as the NCC originating in the Baltic Sea around 58°N flowing northward along the coast all the way to its final destination in the Barents Sea. In comparison with NorKyst800, $C2_{EGG}$ shows a slightly larger ~7 cm standard deviation of differences than the other two geodetic MDTs (~6 cm), see supporting information Table S4. All geodetic MDTs show areas along the coast with smaller values than expected. For example, a fall toward the coast between 65 and 70°N, as well as along the northeastern coast, is evident in all geodetic MDTs, although with slight variations. The most striking coastal feature of $C2_{EGG}$ and $C2_{NMA}$ is an MDT low seen in the area between the Lofoten-Vesterålen area and Senja island, roughly at 69°N, between 15 and 20°E. This feature is much less visible in $C2_{NKG}$.

The ocean and geodetic MDT profiles at TGs are shown in Figure 2. The coastal MDT profile obtained from NorKyst800 is smoother compared to the MDT profiles obtained from TGs and CS2. In accordance with the findings of *Ophaug et al.* [2015], we observe a 10 cm rise toward Kabelvåg, a flattening toward Stavanger, and another 10 cm rise toward Viker. We note the largest differences in the Lofoten-Vesterålen area (~10 cm). The geodetic MDTs show a large spread at Hammerfest, Andenes, and Bodø, but agree well at Honningsvåg, Mausund, Heimsjø, and Stavanger. We further observe a polarization of TG and CS2 MDTs at some TGs. At Tromsø, Rørvik, and Ålesund the TG MDTs agree more with NorKyst800 than the CS2 MDTs, while the converse holds true at Bodø and Bergen. In comparison with their respective TG MDT, $C2_{NKG}$, $C2_{EGG}$, and $C2_{NMA}$ show profile standard deviations of differences of 4.5 cm, 4.7 cm, and 3.9 cm, respectively. In comparison with NorKyst800, $C2_{NKG}$, $C2_{EGG}$, and $C2_{NMA}$ show values of 3.6 cm, 3.4 cm, and 3.2 cm, respectively. TG_{NKG}, TG_{EGG}, and TG_{NMA} show profile standard deviations of differences of 4.1 cm, 4.7 cm, and 3.9 cm to NorKyst800, respectively. We regard these numbers as promising considering previous studies of coastal MDT, which have shown an agreement between tide-gauge geodetic and ocean MDTs on the ~2–14 cm level [e.g., *Woodworth et al.*, 2012; *Higginson et al.*, 2015; *Lin et al.*, 2015; *Ophaug et al.*, 2015; *Woodworth et al.*, 2015], and between altimetric geodetic and ocean MDT on the ~5–11 cm level [e.g., *Ophaug et al.*, 2015; *Woodworth et al.*, 2015].

To facilitate the MDT diagnostics, we derived geostrophic velocity fields, see supporting information Text S1 and Figure 3. Prior to the differentiation, all MDTs were slightly filtered using a Gaussian kernel with a filter width of 12 km. The general pattern of the Norwegian Sea circulation is evident in NorKyst800, $C2_{NKG}$, and $C2_{NMA}$. We trace the NwASC northward and observe its branching at the Barents Sea Opening around 72°N, as well as the hot spots at Svinøy around 62.5°N and the Lofoten-Vesterålen area. We also see the NCC originating in the Baltic Sea around 58°N, flowing northward, splitting from the NwASC at Svinøy and connecting with it again in the Lofoten-Vesterålen area, and continuing toward the Barents Sea. The strongest and most

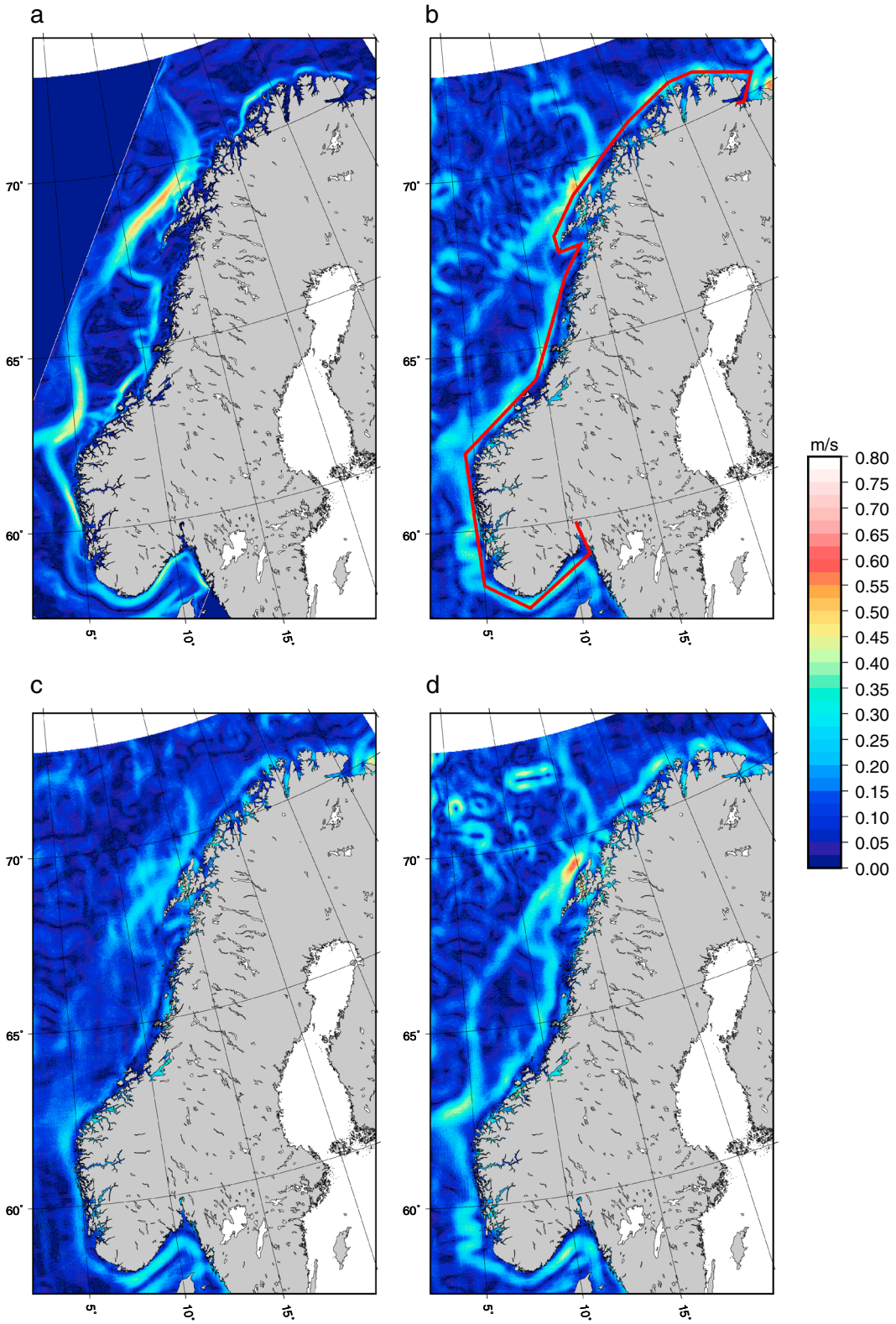

Figure 3. Geostrophic ocean surface currents derived from (a) NorKyst800, (b) $C2_{NKG}$, (c) $C2_{EGG}$, and (d) $C2_{NMA}$. The red line in Figure 3b shows the CS2 SARIn mode border, using the geographical mode mask version 3.8 [*ESA*, 2016].

well-defined currents are visible in NorKyst800, which are highly correlated with the bathymetry (compare with Figure 1a). $C2_{NMA}$ shows the strongest currents and most distinct pattern of the geodetic MDTs, followed closely by $C2_{NKG}$. $C2_{EGG}$ also shows the NCC, but the open-ocean circulation pattern is more or less absent, apart from the hot spot in the Lofoten-Vesterålen area.

By considering the geostrophic surface current patterns, we try to distinguish dynamical features that are actual ocean signal from artificial features related to errors in the marine gravity field. As noted for $C2_{EGG}$ and $C2_{NMA}$, we see the MDT lows in the area between Lofoten-Vesterålen and Senja island translate into small currents. In addition, we observe several eddy-like current features in $C2_{NMA}$ north of 70°N, between 5 and 15°E, which are much less prominent in $C2_{NKG}$, and not visible in $C2_{EGG}$. Thus, they are likely to be artificial ocean signal related to geoid errors. On the other hand, the eddy feature with a center at 69°N, 4°E is visible in all geodetic MDTs and is most prominent in $C2_{NKG}$. This feature is the so-called Lofoten Vortex, a major quasi-permanent mesoscale eddy in the Nordic Seas [*Raj et al.*, 2015]. We note two prominent current signals in $C2_{NKG}$ and $C2_{NMA}$ south of 60°N and west of 5°E which are not seen in $C2_{EGG}$ but tend to be present in NorKyst800 and therefore possibly related to actual ocean signal. Finally, the transition zone between the CS2 geographical mask modes seems to translate into a current which largely follows the path of the NCC. This effect is most prominent in $C2_{EGG}$, where the ocean signal is weaker and less visible in $C2_{NKG}$ and $C2_{NMA}$.

4. Summary and Discussion

In this work, we have shown the promising abilities of CS2 SAR(In) altimetry to recover MDT closer to the Norwegian coast than conventional altimetry, even in skerry landscapes and fjords. At tide gauges, the CS2 MDTs agree on the ∼3–5 cm level with both tide-gauge and ocean MDTs, which are determined using fundamentally different methods. We determine geostrophic surface currents to further assess the MDTs, as both ocean and artificial signals are enhanced through the differentiation. The general circulation pattern is revealed in the geodetic MDTs. However, in spite of these encouraging results, our CS2 MDTs show different artifacts related to the resolution and accuracy of the marine geoid. These variations are observed even though we have restricted ourselves to using new high-resolution gravimetric geoid models which are all based on the same satellite gravity information. This suggests that there is significant MDT signal at smaller spatial scales than those resolved by GOCE, and that the geodetic MDT can be improved by considering regional geoid models which include terrestrial gravity data.

As mentioned in section 3, Figure 2 reveals a polarization of TG and CS2 MDTs at some sites. In some cases, the TG MDTs agree more with NorKyst800 than the CS2 MDTs. As all geodetic MDTs are based on the same geoid models, this suggests that the CS2 MDTs are off due to noisy CS2 targets rather than geoid errors. Using the same argument, in case the CS2 MDTs agree more with NorKyst800 than the TG MDTs, this suggests that there could be an error in the ellipsoidal height of MSL. Our method for determining the ellipsoidal height of MSL at the tide gauges makes these values dependent on HREF accuracy, which in turn is dependent on GNSS/leveling and errors in the geoid it is based on. We continue to stress that ellipsoidal heights at tide gauges are best determined directly by GNSS, simplifying the error budget of the geodetic MDT.

The three regional geoid models in this work are mostly based on the same terrestrial gravity data. Therefore, varying data, weighting and interpolation methods used for their determination are likely to affect the observed variation in the geodetic MDTs. NKG2015 and NMA2014 are both almost completely free of altimetry-derived gravity information (and thus independent of the altimetry observations they are subtracted from). They differ in that the terrestrial gravity database has been updated for NKG2015, and a different gravity interpolation technique was used for its determination. In general, gravity data are sparse in a small coastal gap between observations on land and on the open ocean, which might affect the gravity interpolation there. The MDT low in $C2_{NMA}$ in the area between Lofoten-Vesterålen and Senja, mentioned in section 3, is likely due to a gravity data interpolation issue in the computation of NMA2014, as gravity data are sparse in this particular area (O. C. D. Omang, NMA, personal communication, 2016). This seems to have been resolved in the more recent NKG2015. Furthermore, the eddy-like current features in $C2_{NMA}$ might be linked to undetected systematics in shipborne gravity in that area, which have been addressed in NKG2015. EGG2015 differs from NKG2015 and NMA2014 in that it is heavily based on altimetry-derived gravity. Looking at Figure 3c, we note that the branching of the NwASC is less emphasized in $C2_{EGG}$, and north-south flows generally seem less distinct. The prominent current signals in $C2_{NKG}$ and $C2_{NMA}$ which are slightly correlated with the current seen in NorKyst800 are not seen in $C2_{EGG}$. This could, in part, be owing to the way gravity is derived from altimetry.

Another challenge is posed by the geographical mode mask of CS2. The SARIn mode only stretches out to roughly ~40 km off the coast, where it blends into the LR or SAR mode. In addition, being more sparse at the border, the SARIn and LRM/SAR observations are also more uncertain in this area, as SIRAL is in the process of switching modes. Notably, in $C2_{EGG}$, the border area gives an artificial contribution to the NCC. $C2_{NKG}$ and $C2_{NMA}$ are less affected. EGG2015 has a slightly coarser resolution than NKG2015 and NMA2014 and is expected to be smoother due to the incorporation of altimetry-derived gravity. This might be a reason why the artificial signal caused by the CS2 geographical mode mask is emphasized in $C2_{EGG}$. As the CS2 geographical mask border largely coincides with the NCC, the combination of CS2 modes will always require special attention in studies of Norwegian coastal dynamics. This suggests that in the future, the SARIn mask should stretch further out from the coast than it presently does.

Finally, our CS2 MDTs are based on novel SARIn processing and data screening. Our editing of the CS2 SARIn data is crude, and only ~55% of the raw CS2 data (omitting points on land) are used. This not only suggests that a considerable amount of valid data points did not pass the editing but also reveals that the CS2 targets along the Norwegian coast are generally noisy. Also, a large amount of CS2 observations inside fjords do not have a valid ocean tide (OT) correction, as they are outside the coverage of the standard global OT model. These observations have been disregarded in this work but could be included in the future by considering local ocean tide corrections [*Idžanović et al.*, 2016].

At this point, we would like to stress that NorKyst800 errors also form a component of our MDT error estimates. Using the simple error budgeting approach of *Ophaug et al.* [2015], which relates the empirical standard deviation of differences to the formal error propagation, we get a 2–3 cm error contribution from NorKyst800. Thus, we have used our MDT profile standard deviations and assume equal error contributions from ellipsoidal sea level, geoid model, and NorKyst800.

We have shown that by using oceanographic results, we are able to constrain the regional geoid models, and for the first time we are able to identify errors in the regional geoid models through this approach. Using the traditional external geoid validation method by comparison with GNSS/leveling, we would not be able to unveil artifacts related to systematics in old shipborne marine gravity data or marine gravity data gaps.

At the current stage our results highlight the great improvement in coastal MDT determination due to new regional geoid models and the SAR(In) altimeter on board CS2. The continued improvement of the former remains decisive for the coastal MDT. We relate the main improvement of the latter to the smaller SAR footprint, giving valid observations closer to the coast than conventional altimeters. As such, this study has implications for new-generation SAR altimetry such as the Sentinel-3 and Jason-CS/Sentinel-6 missions of ESA, European Organisation for the Exploitation of Meteorological Satellites, NASA, and NOAA.

Acknowledgments
We acknowledge the open data policy of ESA, MET Norway, PSMSL, and RADS. We would like to thank K. Breili at the Norwegian Mapping Authority for providing data and helpful comments. Figures were drafted using GMT. Data used to produce Figures 1–3 and supporting information Table S4 are available upon request. O. B. Andersen was supported by the European Space Agency's GOCE++DYCOT project. This work is part of the Norwegian University of Life Science's GOCODYN project, supported by the Norwegian Research Council under project number 231017. Finally, we would like to thank two anonymous reviewers for helpful comments that greatly improved the manuscript.

References

Abulaitijiang, A., O. B. Andersen, and L. Stenseng (2015), Coastal sea level from inland CryoSat-2 interferometric SAR altimetry, *Geophys. Res. Lett.*, *42*, 1841–1847, doi:10.1002/2015GL063131.

Ågren, J., et al. (2016), On the development of the new Nordic gravimetric geoid model NKG2015, paper presented at the IAG Symposium on Gravity, Geoid and Height Systems, Thessaloniki, Greece, 19–23 Sept.

Armitage, T. W. K., and M. W. J. Davidson (2014), Using the interferometric capabilities of the ESA CryoSat-2 mission to improve the accuracy of sea ice freeboard retrievals, *IEEE Trans. Geosci. Remote Sens.*, *52*(1), 529–536, doi:10.1109/TGRS.2013.2242082.

Benveniste, J., A. Ambrózio, M. Restano, and S. Dinardo (2016), SAR processing on demand service for CryoSat-2 and Sentinel-3 at ESA G-POD. Geophysical Research Abstracts vol. 18, EGU2016-13084 presented at 2016 EGU General Assembly, Vienna Austria, 17–22 Apr.

Budgell, W. P. (2005), Numerical simulation of ice-ocean variability in the Barents Sea region. Towards dynamical downscaling, *Ocean Dyn.*, *55*(3), 370–387, doi:10.1007/s10236-005-0008-3.

Cartwright, D. E., and A. C. Edden (1973), Corrected tables of tidal harmonics, *Geophys. J. Int.*, *33*(3), 253–264, doi:10.1111/j.1365-246X.1973.tb03420.x.

Cartwright, D. E., and R. J. Tayler (1971), New computations of the tide-generating potential, *Geophys. J. Int.*, *23*(1), 45–73, doi:10.1111/j.1365-246X.1971.tb01803.x.

Chelton, D. B., J. C. Ries, B. J. Haines, L.-L. Fu, and P. S. Callahan (2001), Chapter 1 satellite altimetry, in *Satellite Altimetry and Earth Sciences—A Handbook of Techniques and Applications*, edited by L.-L. Fu and A. Cazenave, pp. 1–131, Academic Press, San Diego, Calif., doi:10.1016/S0074-6142(01)80146-7.

Dee, D. P., et al. (2011), The ERA-Interim reanalysis: Configuration and performance of the data assimilation system, *Q. J. R. Meteorol. Soc.*, *137*, 553–597, doi:10.1002/qj.828.

Denker, H. (2013), Regional gravity field modeling: Theory and practical results, in *Sciences of Geodesy—II*, edited by G. Xu, pp. 185–291, Springer, Berlin, doi:10.1007/978-3-642-28000-9_5.

Denker, H. (2016), A new European gravimetric (quasi)geoid EGG2015, paper presented at the IAG Symposium on Gravity, Geoid and Height Systems, Thessaloniki, Greece, 19–23 Sept.

Drinkwater, M. R., R. Floberghagen, R. Haagmans, D. Muzi, and A. Popescu (2003), GOCE: ESA's first Earth Explorer Core mission, in *Earth Gravity Field from Space—From Sensors to Earth Sciences*, edited by G. Beutler et al., pp. 419–432, Springer, Netherlands. Space Sci. Ser. of ISSI., doi:10.1007/978-94-017-1333-7_36.

Egbert, G. D., and S. Y. Erofeeva (2002), Efficient inverse modeling of barotropic ocean tides, *J. Atmos. Oceanic Technol.*, *19*, 183–204, doi:10.1175/1520-0426(2002)019<0183:EIMOBO>2.0.CO;2.

Ekman, M. (1989), Impacts of geodynamic phenomena on systems for height and gravity, *Bull. Geod.*, *63*(3), 281–296, doi:10.1007/BF02520477.

European Space Agency (2016), Geographical mode mask. [Available at https://earth.esa.int/web/guest/-/geographical-mode-mask-7107, last accessed 27 April 2016.]

European Space Research Institute (ESRIN) – European Space Agency, and Mullard Space Science Laboratory – University College London (2012), CryoSat product handbook, London, U. K. [Available at: http://emits.sso.esa.int/emits-doc/ESRIN/7158/CryoSat-PHB-17apr2012.pdf, last accessed 29 May 2017.]

Forsberg, R., and C. C. Tscherning (2008), An Overview Manual for the GRAVSOFT Geodetic Gravity Field Modelling Programs, 2nd ed., Contract Report to JUPEM, Copenhagen, Denmark. [Available at: http://cct.gfy.ku.dk/publ_cct/cct1792.pdf, last accessed 29 May 2017.]

Haidvogel, D. B., et al. (2008), Ocean forecasting in terrain-following coordinates: Formulation and skill assessment of the Regional Ocean Modeling System, *J. Comput. Phys.*, *227*(7), 3595–3624, doi:10.1016/j.jcp.2007.06.016.

Higginson, S., K. R. Thompson, P. L. Woodworth, and C. W. Hughes (2015), The tilt of mean sea level along the east coast of North America, *Geophys. Res. Lett.*, *42*, 1471–1479, doi:10.1002/2015GL063186.

Holgate, S. J., A. Matthews, P. L. Woodworth, L. J. Rickards, M. E. Tamisiea, E. Bradshaw, P. R. Foden, K. M. Gordon, S. Jevrejeva, and J. Pugh (2013), New data systems and products at the Permanent Service for Mean Sea Level, *J. Coastal Res.*, *29*(3), 493–504, doi:10.2112/jcoastres-d-12-00175.1.

Hughes, C. W., R. J. Bingham, V. Roussenov, J. Williams, and P. L. Woodworth (2015), The effect of Mediterranean exchange flow on European time mean sea level, *Geophys. Res. Lett.*, *42*, 466–474, doi:10.1002/2014GL062654.

Idžanović, M., V. Ophaug, and O. B. Andersen (2016), Coastal sea level in Norway from CryoSat-2 SAR altimetry, paper presented at 2016 European Space Agency Living Planet Symposium, ESA Special Publication SP-740 on CD-ROM, Prague, Czech Republic, 9–13 May.

Koch, K.-R. (1999), *Parameter Estimation and Hypothesis Testing in Linear Models*, Springer, Berlin.

Lin, H., K. R. Thompson, J. Huang, and M. Véronneau (2015), Tilt of mean sea level along the Pacific coasts of North America and Japan, *J. Geophys. Res. Oceans*, *120*, 6815–6828, doi:10.1002/2015JC010920.

Moritz, H. (1980), *Advanced Physical Geodesy*, Herbert Wichmann, Karlsruhe, Germany.

Ophaug, V., K. Breili, and C. Gerlach (2015), A comparative assessment of coastal mean dynamic topography in Norway by geodetic and ocean approaches, *J. Geophys. Res. Oceans*, *120*, 7807–7826, doi:10.1002/2015JC011145.

Pugh, D., and P. L. Woodworth (2014), *Sea-Level Science: Understanding Tides, Surges, Tsunamis and Mean Sea-Level Changes*, Cambridge Univ. Press, Cambridge, U. K.

Raj, R. P., L. Chafik, J. E. Ø. Nilsen, T. Eldevik, and I. Halo (2015), The Lofoten vortex of the Nordic seas, *Deep Sea Res, Part I*, *96*, 1–14, doi:10.1016/j.dsr.2014.10.011.

Ray, C., C. Martin-Puig, M. P. Clarizia, G. Ruffini, S. Dinardo, C. Gommenginger, and J. Benveniste (2015), SAR altimeter backscattered waveform model, *IEEE Trans. Geosci. Remote Sens.*, *53*(2), 911–919, doi:10.1109/TGRS.2014.2330423.

Røed L. P., and J. Debernard (2004), Description of an integrated flux and sea-ice model suitable for coupling to an ocean and atmosphere model, Meteorol. No Rep. 4/2004, 56 pp., Norwegian Meteorol. Inst., Oslo, Norway.

Scharroo, R., E. W. Leuliette, J. L. Lillibridge, D. Byrne, M. C. Naeije, and G. T. Mitchum (2013a), RADS: Consistent multimission products, paper ESA SP-710 presented at Symposium on 20 Years of Progress in Radar Altimetry, ESA Special Publication, Venice, Italy, 20–28 Sep.

Scharroo, R., W. H. F. Smith, E. W. Leuliette, and J. L. Lillibridge (2013b), RADS: The performance of CryoSat as an ocean altimeter. Paper ESA SP-717 presented at 3rd CryoSat-2 User Workshop, ESA Special Publication, Dresden, Germany, 12–14 Mar.

Simpson, M. J. R., J. E. Ø. Nilsen, O. R. Ravndal, K. Breili, H. Sande, H. P. Kierulf, H. Steffen, E. Jansen, M. Carson, and O. Vestøl (2015), Sea level change for Norway: Past and present observations and projections to 2100, Norwegian Cent. for Clim. Serv. Rep. 1/2015, Norwegian Cent. for Clim. Serv., Oslo, Norway.

Solheim, D. (2000), New height reference surfaces for Norway, in *Report on the Symposium of the IAG Subcommission for Europe (EUREF) in Tromsø, 22–24 Jun.*, edited by J. A. Torres and H. Hornik, pp. 154–158, Verlag der Bayerischen Akademie der Wissenschaften, Munich, Germany.

Vignudelli, S., A. G. Kostianoy, P. Cipollini, and J. Benveniste (Eds.) (2011), Coastal altimetry,Springer, Berlin, doi:10.1007/978-3-642-12796-0.

Wahr, J. M. (1985), Deformation induced by polar motion, *J. Geophys. Res.*, *90*(B11), 9363–9368, doi:10.1029/JB090iB11p09363.

Weatherall, P., K. M. Marks, M. Jakobsson, T. Schmidt, S. Tani, J. E. Arndt, M. Rovere, D. Chayes, V. Ferrini, and R. Wigley (2015), A new digital bathymetric model of the world's oceans, *Earth Space Sci.*, *2*, 331–345, doi:10.1002/2015EA000107.

Wessel, P., W. H. F. Smith, R. Scharroo, J. Luis, and F. Wobbe (2013), Generic mapping tools: Improved version released, *Eos Trans. AGU*, *94*(45), 409–410, doi:10.1002/2013EO450001.

Wingham, D. J., et al. (2006), CryoSat: A mission to determine the fluctuations in Earth's land and marine ice fields, *Adv. Space Res.*, *37*(4), 841–871, doi:10.1016/j.asr.2005.07.027.

Woodworth, P. L., C. Hughes, R. J. Bingham, and T. Gruber (2012), Towards worldwide height system unification using ocean information, *J. Geod. Sci.*, *2*(4), 302–318, doi:10.2478/v10156-012-0004-8.

Woodworth, P. L., M. Gravelle, M. Marcos, G. Wöppelmann, and C. W. Hughes (2015), The status of measurement of the Mediterranean mean dynamic topography by geodetic techniques, *J. Geod.*, *89*(8), 811–827, doi:10.1007/s00190-015-0817-1.

Wunsch, C., and D. Stammer (1997), Atmospheric loading and the oceanic "inverted barometer" effect, *Rev. Geophys.*, *35*(1), 79–107, doi:10.1029/96RG03037.

Wunsch, C., and D. Stammer (1998), Satellite altimetry, the marine geoid, and the oceanic general circulation, *Annu. Rev. Earth Planet. Sci.*, *26*, 219–253, doi:10.1146/annurev.earth.26.1.219.